Secondary source and error sensing strategies for the active control of sound transmission through a small opening

Congxin Zhang [a], Ming Qin [a], Haishan Zou [a,*], Xiaojun Qiu [b]

[a] Key Laboratory of Modern Acoustics and Institute of Acoustics, Nanjing University, Nanjing 210093, China.

[b] Centre for Audio, Acoustics and Vibration, Faculty of Engineering and IT, University of Technology Sydney, Sydney, NSW 2007, Australia

* Corresponding author.
E-mail address: hszou@nju.edu.cn (H. Zou)

ABSTARCT

The openings of an enclosure allow natural ventilation and light ingress but also act as a point of entry for noise of the whole structure. In this paper, the active control of the sound transmitted through a small opening in a wall formed by two infinitely-large baffles is investigated up to 4000 Hz. Based on an analytical model developed with the modal expansion method, the effects of different secondary source and the error sensor strategies are compared numerically for different types of primary sound fields. The upper limit frequency of effective control is found to be determined by the eigen frequency of the acoustic modes of the opening. Experimental results with an opening of 6 cm by 6 cm on a 31.8 cm thick wall agree well with the numerical results. The upper limit frequency of effective control is found to be 2750 Hz for a single-channel system and 3900 Hz for a 4-channel system with more than 10 dB noise reduction. It is concluded that implementing active control in small openings with appropriate secondary source and error sensing strategy can extend the frequency range of control significantly, so that the active control systems can be applied to more noise control scenarios which have both noise reduction and ventilation requirements in the middle to high frequency range.

Key words: small opening; sound transmission; active noise control; control strategy

1. Introduction

The openings of an enclosure such as windows, doors and ventilation ducts allow natural ventilation and light ingress but also act as a point of entry for noise of the whole structure. Much research has gone into the prediction of sound transmission through apertures to aid in the investigation of passive and active noise control measures.

Different models have been proposed for analyzing the sound transmission through an opening in a wall. Earlier studies had focused on circular openings in infinitely large walls. With the boundary conditions established by using integral equations, the transmission coefficient of the opening was expressed as a function of ka (where k is the wave number and a is the aperture radius), and the transmission coefficient was found to be independent of ka at low frequencies and approach unity at high frequencies [1]. These studies have been extended to openings in a wall with arbitrary thickness, and an approximate solution was proposed by combining the piston theory with the plane wave assumption inside the opening [2]. The experimental results between two reverberant chambers indicate that the error of the solution is on average less than 2 dB up to $ka = 8$, where the plane wave assumption becomes invalid. The case of a rectangular opening under similar boundary conditions was also investigated and the square apertures were found to behave similarly to the circular ones [3].

Some numerical models have been developed for complicated sound fields. To predict the sound transmission loss of openings in a diffuse field, a numerical method based on the modal expansion has been presented, being validated by the FEM-BEM and experiments [4]. Another model has been presented by using a spatial Fourier transform approach to obtain the scattered and transmitted fields in series forms [7]. For a point source impinging from at an arbitrary angle in the far field, an approximate model has been proposed. The model ignores the coupling of the higher-order modes, so becomes invalid when the point source is near the opening [9]. The interaction between an opening and its adjacent rooms with the oblique incidence point source has been considered, but this method requires large amount of computation when accounting for the eigenmodes in both rooms [10]. However, the numerical methods introduce an integral which converges slowly and contains troublesome singularities. To improve the accuracy and numerical efficiency of the transmission model for a cylindrical opening, a rigorous model with highly convergent hypergeometric series in terms of a Hankel transform has been proposed [11].

Passive methods have been applied in reducing noise transmitted through openings of a building due to their stability and ease of design for a certain kind of noise. A quarter-wave resonator was designed to attenuate fan noise entering buildings through openings and obtained approximately 6–7 dB attenuation in the 1.25 and 3.15 kHz one-third octave bands [12]. By designing resonators of different lengths, noise attenuation over a wide frequency range rather than at an isolated, discrete frequency can be achieved. However, the volume of the resonator is large for low frequency noise for the length of the resonator corresponds to one quarter wavelength or odd multiple of the noise. The transparent micro-perforated absorbers were used along the ventilation path of a staggered window to control road traffic noise and obtained approximate 5.8 dB in the 800–8000 Hz range [13]. This method allows noise attenuation whilst maintaining comfort ventilation and daylighting. However, the limitations include poor noise reduction at low frequencies, the ventilation performance being limited by the staggered structure, and extra space for multiple layers of MPA.

In order to improve noise reduction performance at low frequencies, active noise control (ANC) technique has been applied in the openings. To reduce noise radiated outward from a room through a window, a multichannel ANC system with 5 secondary sources in the surrounding wall and 4 error sensors in the opening was developed and a noise reduction of 15 dB was achieved in the 200 Hz one-third octave band [14]. To block the noise from a window of 0.09 m^2 into a room, an 8-channel active window system with its control sources evenly distributed at the edge of the window was established and a noise reduction of approximate 10 dB was achieved in the range of 400–1000 Hz [15].

Lots of channels are needed for a relatively large window. A 16-channel ANC system with secondary sources distributed evenly on the opening was tested with a full-sized window, and an overall attenuation of more than 5 dB below 2000 Hz was achieved [16]. Another solution is using the double layers sound insulation structures with staggered opening, and ANC systems are developed to combine with such structures to form the hybrid noise control systems. For example, the secondary source was embedded in a staggered ventilation duct for the window, and a noise reduction of 10 dB at observation points was achieved up to 390 Hz for a single-channel system and 420 Hz for a 2-channel system in the experiments [17]. This solution transforms the original three dimensional sound field problems into one dimensional duct acoustic problems so that ANC can be applied more efficiently with better noise reduction performance and lower cost. Its disadvantages are the complicated structure and some loss of the air exchange rate.

The mechanisms and secondary source configurations of an ANC system for large openings have been discussed. Three mechanisms were revealed to act together in reducing the sound radiation through the opening, which include changing the impedance of the primary source, modal control and modal rearrangement [18]. The size of an opening affects the control performance. When the opening size is compatible with the acoustic wavelength, a few sources are necessary for good control, but when the size is large compared to the wavelength, more secondary sources are required for good control and the results become similar to those in the free-field [19]. Different physical arrangements of control sources in a window with planar wave incidence were investigated using a 2D FEM model [20]. It was found that the array of secondary sources exhibited good overall performance when situated in the center of the walls and the separation distance between the secondary sources should be less than $\lambda/(1+\sin\theta)$ (where λ is the wave length and θ is the angle of incidence).

Presently, the models for predicting the opening transmission in a wall with arbitrary thickness have been established, passive methods have been proposed to reduce sound transmission through openings at high frequencies, and active control systems have been applied in large openings in the low frequency range. Considering the requirement of natural ventilation and noise reduction for buildings, it is a feasible solution for installing ANC systems in several small openings in the outer wall. The straight and short opening without staggered structure is good for ventilation at the cost of almost no noise reduction effect. In addition, since the passive method requires more space or reduces ventilation, only active control but not hybrid control is adopted. As a result, the frequency range of effective noise reduction of the ANC system should be extended to middle and high frequency range, such as up to 4000 Hz, which covers most of the frequency bands of traffic noise and environmental noise. In this paper, an ANC system in a small opening is investigated. An analytical model was first developed to analyze the effects of different secondary source and the error sensor strategies. Simulations with analytical model agree with the FEM method. Finally, the experiments were designed in an anechoic chamber which verify the proposed analytical models and show the practical feasibility of the active control system in a small opening. For more ventilation, multiple openings containing active control systems can be designed on the wall, so the wall can reduce the noise transmitted through the openings with good natural ventilation.

2. Analytical model

Fig. 1 shows a rectangular opening in a wall formed by two infinitely-large baffles with the length, width and depth of L_x, L_y, and t, respectively. A primary source is located outside the opening, and a secondary source is located in the opening within the depth of the wall, both of which are point monopole sources. The Cartesian coordinate system is established with the origin at the center of the opening on the incidence side.

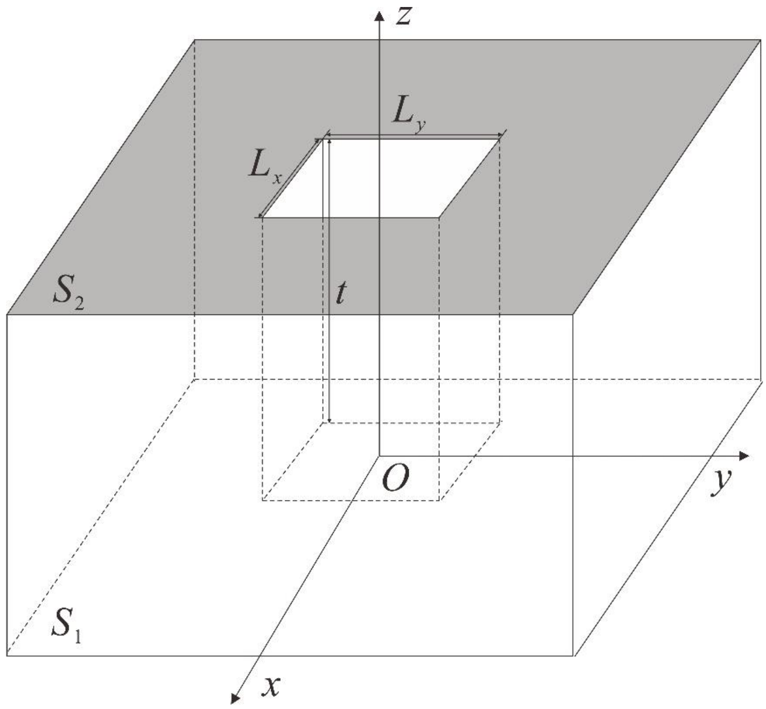

(a)

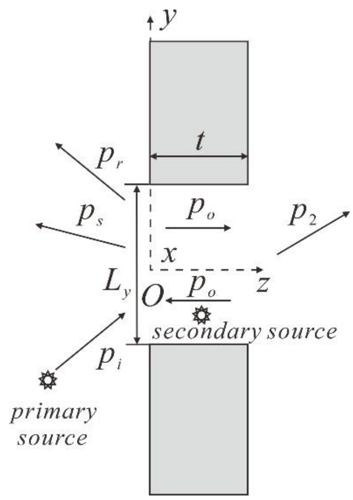

(b)

Fig. 1. An opening in an infinitely large wall, (a) three-dimensional view of the opening, (b) acoustic scattering and transmission of the opening.

2.1. The primary sound field

As shown in Fig. 1, the sound pressure at the incidence side of the opening can be calculated by the sum of the incident sound pressure p_i, the reflected sound pressure p_r, and the scattered sound pressure p_s as [4]

$$p_1(\mathbf{r}) = p_i(\mathbf{r}) + p_r(\mathbf{r}) + p_s(\mathbf{r}), \tag{1}$$

where $\mathbf{r} = (x, y, z)$ is a location in the sound field, and

$$p_i(\mathbf{r}) = \frac{\mathrm{j}\omega\rho q_p}{4\pi\left|\mathbf{r}-\mathbf{r}_p\right|}\mathrm{e}^{-\mathrm{j}k\left|\mathbf{r}-\mathbf{r}_p\right|}, \tag{2}$$

$$p_r(\mathbf{r}) = \frac{\mathrm{j}\omega\rho q_p}{4\pi\left|\mathbf{r}-\mathbf{r}'_p\right|}\mathrm{e}^{-\mathrm{j}k\left|\mathbf{r}-\mathbf{r}'_p\right|}, \tag{3}$$

$$p_s(\mathbf{r}) = -\int_{S_1} G(\mathbf{r},\mathbf{r}_1)\frac{\partial p_s(\mathbf{r}_1)}{\partial z}\mathrm{d}s, \tag{4}$$

where j denotes the imaginary unit, k is the wave number, ω is the angular frequency, ρ is the density of the medium and q_p is the strength of the primary source. $\mathbf{r}_p = (x_p, y_p, z_p)$ and $\mathbf{r}'_p = (x_p, y_p, -z_p)$ are the coordinates of the primary source and its mirror image of the wall.

The incidence side of the opening surface is marked S_1, $\mathbf{r}_1 = (x_1, y_1, 0)$ is a location on S_1, and $G(\mathbf{r}, \mathbf{r}_1)$ is the Green function in the semi-infinite space given by

$$G(\mathbf{r},\mathbf{r}_1) = \frac{\mathrm{e}^{-\mathrm{j}k\left|\mathbf{r}-\mathbf{r}_1\right|}}{2\pi\left|\mathbf{r}-\mathbf{r}_1\right|}. \tag{5}$$

The acoustic field inside the opening can be expanded analytically from [4]

$$p_o(\mathbf{r}) = \sum_{m=0}^{\infty}\left[A_m\mathrm{e}^{-\mathrm{j}k_m z} + B_m\mathrm{e}^{\mathrm{j}k_m z}\right]\phi_m(x,y), \tag{6}$$

where A_m and B_m are the amplitudes of the mth mode propagating in the positive and negative z directions inside the opening. The wave number k_m and k are related by

$$k_m = \sqrt{k^2 - \left(\frac{m_x\pi}{L_x}\right)^2 - \left(\frac{m_y\pi}{L_y}\right)^2}, \tag{7}$$

where m_x and m_y are the modal indices. $\phi_m(x, y)$ is the eigenfunction of the (m_x, m_y)

mode of an infinitely long rectangular rigid duct with a cross section of $L_x \times L_y$, which is given by

$$\phi_m(x, y) = \cos\left[\frac{m_x \pi}{L_x}\left(x + \frac{L_x}{2}\right)\right]\cos\left[\frac{m_y \pi}{L_y}\left(y + \frac{L_y}{2}\right)\right]. \tag{8}$$

Similarly, the sound pressure at the transmitted side can be expressed as

$$p_2(\mathbf{r}) = \int_{S_2} G(\mathbf{r}, \mathbf{r}_2)\frac{\partial p_2(\mathbf{r}_2)}{\partial z}\mathrm{d}s, \tag{9}$$

where S_2 is the opening surface on the transmitted side, and $\mathbf{r}_2 = (x_2, y_2, t)$ is a location on S_2.

The boundary conditions on both end surfaces of the opening are [4]

$$p_1(\mathbf{r})\big|_{z=0} = p_o(\mathbf{r})\big|_{z=0}, \tag{10a}$$

$$\left.\frac{\partial p_1(\mathbf{r})}{\partial z}\right|_{z=0} = \left.\frac{\partial p_o(\mathbf{r})}{\partial z}\right|_{z=0}, \tag{10b}$$

$$p_2(\mathbf{r})\big|_{z=t} = p_o(\mathbf{r})\big|_{z=t}, \tag{11a}$$

$$\left.\frac{\partial p_2(\mathbf{r})}{\partial z}\right|_{z=t} = \left.\frac{\partial p_o(\mathbf{r})}{\partial z}\right|_{z=t}. \tag{11b}$$

By substituting Eqs. (1), (6) and (9) into Eqs. (10) and (11), multiplying both sides of the equations with ϕ_n, and integrating on both end surfaces of the opening, yields

$$\frac{L_x L_y}{\omega\rho}\sum_{n=0}^{\infty} k_n(-A_n + B_n)Z_{mn} = (A_m + B_m)N_m^2 - F_m, \tag{12}$$

$$-\frac{L_x L_y}{\omega\rho}\sum_{n=0}^{\infty} k_n\left(-A_n \mathrm{e}^{-\mathrm{j}k_n t} + B_n \mathrm{e}^{\mathrm{j}k_n t}\right)Z_{mn} = \left(A_m \mathrm{e}^{-\mathrm{j}k_n t} + B_m \mathrm{e}^{\mathrm{j}k_n t}\right)N_m^2, \tag{13}$$

where $N_m{}^2 = \varepsilon_{m_x}\varepsilon_{m_y} L_x L_y / 4$, $\varepsilon_0 = 2$, $\varepsilon_{m_x} = 1$ $(m_x \neq 0)$, $\varepsilon_{m_y} = 1$ $(m_y \neq 0)$, and

$$F_m = \mathrm{j}\omega\rho q_p \int_{-\frac{L_x}{2}}^{\frac{L_x}{2}}\int_{-\frac{L_y}{2}}^{\frac{L_y}{2}} \frac{\mathrm{e}^{-\mathrm{j}k|\mathbf{r}_1 - \mathbf{r}_p|}}{2\pi|\mathbf{r}_1 - \mathbf{r}_p|}\phi_m(x_1, y_1)\mathrm{d}x_1\mathrm{d}y_1, \tag{14}$$

$$Z_{mn} = \frac{\mathrm{j}\omega\rho}{L_x L_y}\int_{-\frac{L_x}{2}}^{\frac{L_x}{2}}\int_{-\frac{L_y}{2}}^{\frac{L_y}{2}}\int_{-\frac{L_x}{2}}^{\frac{L_x}{2}}\int_{-\frac{L_y}{2}}^{\frac{L_y}{2}} \frac{\mathrm{e}^{-\mathrm{j}k_0|\mathbf{r}_0-\mathbf{r}_1|}}{2\pi|\mathbf{r}_0-\mathbf{r}_1|}\phi_m(x_1,y_1)\phi_n(x_0,y_0)\mathrm{d}x_1\mathrm{d}y_1\mathrm{d}x_0\mathrm{d}y_0, \quad (15)$$

where $\mathbf{r}_0 = (x_0, y_0, 0)$, $\mathbf{r}_1 = (x_1, y_1, 0)$, and Z_{mn} is the cross modal radiation impedance between modes m and n [21].

After calculating Eqs. (14) and (15) with numerical methods, A_m and B_m can be obtained by solving Eqs. (12) and (13). Then, the sound pressure at location $\mathbf{r}$ on S_2 can be calculated by substituting Eq. (11b) into Eq. (9), and the corresponding normal particle velocity can be derived by using the sound pressure. The pressure transfer function $Z_{pr}(\mathbf{r}, \mathbf{r}_p)$ and the particle velocity transfer function $Y_{pr}(\mathbf{r}, \mathbf{r}_p)$ from the primary source located at $\mathbf{r}_p$ to location $\mathbf{r}$ on S_2 can be calculated by dividing the sound pressure and the normal particle velocity at the location with the primary source strength.

When K primary sources at locations $\mathbf{r}_{p,1}, \mathbf{r}_{p,2}, \ldots, \mathbf{r}_{p,K}$, are considered, the pressure and the corresponding normal particle velocity of location $\mathbf{r}$ on S_2 can be expressed as

$$p_o(\mathbf{r}) = \mathbf{Z}_{pr}^T(\mathbf{r})\mathbf{q}_p, \quad (16)$$

$$v_{o,z}(\mathbf{r}) = \mathbf{Y}_{pr}^T(\mathbf{r})\mathbf{q}_p, \quad (17)$$

where $\mathbf{q}_p = [q_{p,1}, q_{p,2}, \ldots, q_{p,K}]^T$ is the vector of the K primary sources strengths, $\mathbf{Z}_{pr}(\mathbf{r}) = [Z_{pr}(\mathbf{r}, \mathbf{r}_{p,1}), Z_{pr}(\mathbf{r}, \mathbf{r}_{p,2}), \ldots, Z_{pr}(\mathbf{r}, \mathbf{r}_{p,K})]^T$ and $\mathbf{Y}_{pr}(\mathbf{r}) = [Y_{pr}(\mathbf{r}, \mathbf{r}_{p,1}), Y_{\mathrm{pr}}(\mathbf{r}, \mathbf{r}_{p,2}), \ldots, Y_{pr}(\mathbf{r}, \mathbf{r}_{p,K})]^T$ are the pressure transfer function and the corresponding normal particle velocity transfer function vectors from the primary sources to location $\mathbf{r}$.

The z direction component of the mean acoustic intensity of the primary sources at location $\mathbf{r}$ on the transmitted side of the opening is defined as

$$I_{pz}(\mathbf{r}) = \frac{1}{2}\mathrm{Re}\{p_o(\mathbf{r})v_{o,z}^*(\mathbf{r})\}. \quad (18)$$

Substituting Eqs. (16) and (17) into Eq. (18) and applying the relation $\mathrm{Re}(\mathbf{Z})$ =

(**Z**+**Z***)/2 to the right hand side of Eq. (18) gives

$$I_{pz}(\mathbf{r}) = \frac{1}{4}\mathbf{q}_p^H \left(\mathbf{Y}_{pr}^*(\mathbf{r})\mathbf{Z}_{pr}^T(\mathbf{r}) + \mathbf{Z}_{pr}^*(\mathbf{r})\mathbf{Y}_{pr}^T(\mathbf{r})\right)\mathbf{q}_p . \quad (19)$$

The transmitted sound power from the primary source can be calculated by the integral of the acoustic intensity on the transmitted side surface of the opening, as

$$W_p = \int_{S_2} I_{pz}(\mathbf{r})\mathrm{d}s , \quad (20)$$

which can be expressed in modal amplitudes as

$$W_p = \frac{1}{2\rho\omega}\mathrm{Re}\left\{\sum_{k=1}^{K}\sum_{m=0}^{\infty}\left[A_m(\mathbf{r}_{p,k}) + B_{mk}(\mathbf{r}_{p,k})\right]\left[A_m(\mathbf{r}_{p,k}) - B_{mk}(\mathbf{r}_{p,k})\right]^* k_m^* N_m^2\right\} . \quad (21)$$

2.2. The secondary sound field

For a secondary point source located inside the opening, only the scattered sound wave is generated at the incidence side of the opening and is given by

$$p_1(\mathbf{r}) = -\int_{S_1} G(\mathbf{r},\mathbf{r}_1)\frac{\partial p_s(\mathbf{r}_1)}{\partial z}\mathrm{d}s . \quad (22)$$

The sound pressure at **r** = (x, y, z) inside the opening generated by the secondary source can be expressed as [18]

$$p_o(\mathbf{r}) = \sum_{m=0}^{\infty}\left[U_m \mathrm{e}^{-\mathrm{j}k_m z} + V_m \mathrm{e}^{\mathrm{j}k_m z}\right]\phi_m(x,y) + \int_V \mathrm{j}\omega\rho q_s G_A(\mathbf{r})\mathrm{d}V , \quad (23)$$

where U_m and V_m correspond to the mth amplitudes of the sound propagating in the positive and negative z directions, and q_s is the strength of the secondary source. $G_A(\mathbf{r}, \mathbf{r}_s)$ is the Green's Function from source location $\mathbf{r}_s = (x_s, y_s, z_s)$ to **r** within the depth of the opening, written as [23]

$$G_A(\mathbf{r}) = \frac{-\mathrm{j}}{2}\sum_{m=0}^{\infty}\frac{\phi_m(x,y)\phi_m(x_s,y_s)}{N_m^2 k_m}\mathrm{e}^{-\mathrm{j}k_m|z-z_s|} . \quad (24)$$

Similarly, with Eqs. (22), (23), (9), (10) and (11), the following equations can be derived

$$F_1 = U_m N_m^2 + \sum_{n=0}^{\infty} \mathrm{j} k_n U_n Z_{mn} + V_m N_m^2 - \sum_{n=0}^{\infty} \mathrm{j} k_n V_n Z_{mn} , \tag{25}$$

$$F_2 = U_m \mathrm{e}^{-\mathrm{j}k_m t} N_m^2 + V_m \mathrm{e}^{\mathrm{j}k_m t} N_n^2 - \sum_{n=0}^{\infty} \mathrm{j} k_n U_n \mathrm{e}^{-\mathrm{j}k_n t} Z_{mn} + \sum_{n=0}^{\infty} \mathrm{j} k_n V_n \mathrm{e}^{\mathrm{j}k_n t} Z_{mn} , \tag{26}$$

where

$$F_1 = -\frac{\omega\rho q_s}{2} \cdot \frac{\mathrm{e}^{-\mathrm{j}k_m z_s} \phi_m\left(x_s, y_s\right)}{k_m} - \frac{\omega\rho q_s}{2} \sum_{n=0}^{\infty} \frac{\mathrm{j}\mathrm{e}^{-\mathrm{j}k_n z_s}}{N_n^2} \phi_n\left(x_s, y_s\right) Z_{mn} , \tag{27}$$

$$F_2 = -\frac{\omega\rho q_s}{2} \cdot \frac{\mathrm{e}^{-\mathrm{j}k_m (t - z_s)} \phi_m\left(x_s, y_s\right)}{k_m} - \frac{\omega\rho q_s}{2} \sum_{n=0}^{\infty} \frac{\mathrm{j}\mathrm{e}^{-\mathrm{j}k_n (t - z_s)}}{N_n^2} \phi_n\left(x_s, y_s\right) Z_{mn} . \tag{28}$$

U_m and V_m can be calculated by solving Eqs. (25) and (26), and sound pressure at transmitted side can be calculated by substituting Eq. (11b) into Eq. (9).

2.3. The cost functions

Two different cost functions are considered in the paper, which are the sum of the squared sound pressure at the error sensors and the total transmitted sound power. The first cost function is defined as [24]

$$J_p = \sum_{i=1}^{L} \left| p_{e,i} \right|^2 + \beta \mathbf{q}_s^H \mathbf{q}_s , \tag{29}$$

where L is the number of the error sensors, $p_{e,i}$ is the total sound pressure of the ith error sensor, and $\mathbf{q}_s$ is the vector of the source strengths of the secondary sources. The optimal strengths of the secondary sources can be obtained with [24][24]

$$\mathbf{q}_{s,\mathrm{opt}} = -\left(\mathbf{Z}_{se}^H \mathbf{Z}_{se} + \beta \mathbf{I} \right)^{-1} \mathbf{Z}_{se}^H \mathbf{Z}_{pe} \mathbf{q}_p , \tag{30}$$

where β is a positive real number for constraining the control effort [24]. $\mathbf{Z}_{se}$ is the $L \times M$ matrix of the acoustic transfer functions from the M secondary sources to the L error sensors, and $\mathbf{Z}_{pe}$ is the acoustic transfer functions from the primary sources to the L

error sensors, which can be calculated by the analytical models proposed above.

The second cost function considering the total transmitted sound power can be defined as

$$J_w = \int_{S_2} I_{tz}(\mathbf{r})\mathrm{d}s + \beta \mathbf{q}_s^H \mathbf{q}_s , \tag{31}$$

where $I_{tz}(\mathbf{r})$ is the normal mean acoustic intensity at location $\mathbf{r}$, and can be expressed as [25],

$$\begin{aligned} I_{tz}(\mathbf{r}) &= \mathbf{q}_s^H \left\{ \frac{1}{4}\left[\mathbf{Y}_{sr}^*(\mathbf{r})\mathbf{Z}_{sr}^T(\mathbf{r}) + \mathbf{Z}_{sr}^*(\mathbf{r})\mathbf{Y}_{sr}^T(\mathbf{r}) \right] \right\} \mathbf{q}_s \\ &+ \mathbf{q}_s^H \left\{ \frac{1}{4}\left[\mathbf{q}_p^H \mathbf{Z}_{pr}^*(\mathbf{r})\mathbf{Y}_{sr}^T(\mathbf{r}) + \mathbf{Y}_{pr}^H(\mathbf{r})\mathbf{q}_p^* \mathbf{Z}_{sr}^T(\mathbf{r}) \right] \right\} \\ &+ \left\{ \frac{1}{4}\left[\mathbf{q}_p^H \mathbf{Z}_{pr}^*(\mathbf{r})\mathbf{Y}_{sr}^T(\mathbf{r}) + \mathbf{Y}_{pr}^H(\mathbf{r})\mathbf{q}_p^* \mathbf{Z}_{sr}^T(\mathbf{r}) \right] \right\}^H \mathbf{q}_s + I_{pz}(\mathbf{r}) \end{aligned} , \tag{32}$$

where $\mathbf{Z}_{pr}(\mathbf{r})$ and $\mathbf{Y}_{pr}(\mathbf{r})$ are the pressure transfer function and the particle velocity function from the K primary sources to location $\mathbf{r}$ as defined in Section 2.1, while $\mathbf{Z}_{sr}(\mathbf{r})$ and $\mathbf{Y}_{sr}(\mathbf{r})$ are the M×1 vector of the pressure transfer function and the particle velocity transfer function from the M secondary sources to location $\mathbf{r}$. $I_{pz}(\mathbf{r})$ is the normal mean acoustic intensity of the primary source at the location $\mathbf{r}$, as shown in Eq. (19).

By substituting Eq. (32) into Eq. (31), J_w becomes

$$J_w = \mathbf{q}_s^H \left(\mathbf{A}_w + \beta \mathbf{I} \right) \mathbf{q}_s + \mathbf{q}_s^H \mathbf{b}_w + \mathbf{b}_w^H \mathbf{q}_s + c_w , \tag{33}$$

with

$$\mathbf{A}_w = \int_{S_2} \frac{1}{4}\left[\mathbf{Y}_{sr}^*(\mathbf{r})\mathbf{Z}_{sr}^T(\mathbf{r}) + \mathbf{Z}_{sr}^*(\mathbf{r})\mathbf{Y}_{sr}^T(\mathbf{r}) \right] \mathrm{d}s , \tag{34a}$$

$$\mathbf{b}_w = \int_{S_2} \frac{1}{4}\left[\mathbf{q}_p^H \mathbf{Z}_{pr}^*(\mathbf{r})\mathbf{Y}_{sr}^T(\mathbf{r}) + \mathbf{Y}_{pr}^H(\mathbf{r})\mathbf{q}_p^* \mathbf{Z}_{sr}^T(\mathbf{r}) \right] \mathrm{d}s , \tag{34b}$$

$$c_w = W_p . \tag{34c}$$

By equating $\partial J_w / \partial \mathbf{q}_s$ to 0, the optimal strengths of the M secondary sources $\mathbf{q}_{s,\mathrm{opt}}$

can be obtained as

$$\mathbf{q}_{s,\mathrm{opt}} = -(\mathbf{A}_w + \beta\mathbf{I})^{-1}\mathbf{b}_w . \tag{35}$$

The transmitted sound power with control can be obtained by substituting Eq. (30), Eq. (32) and Eq. (35) into Eq. (20)

$$W_{t,\mathrm{opt}} = \mathbf{q}_{s,\mathrm{opt}}^H \mathbf{A}_w \mathbf{q}_{s,\mathrm{opt}} + \mathbf{q}_{s,\mathrm{opt}}^H \mathbf{b}_w + \mathbf{b}_w^H \mathbf{q}_{s,\mathrm{opt}} + c_w . \tag{36}$$

The performance of the ANC system is defined as the reduction of the transmitted sound power level by

$$\mathrm{NR} = 10\log_{10}\frac{W_p}{W_{t,\mathrm{opt}}} . \tag{37}$$

3. Simulations

3.1. Validation of the analytical model

A rectangular opening with dimensions of L_x = 6 cm, L_y = 6 cm, t = 30 cm is used in the simulations. The thickness of a typical exterior wall of a civil building in China is about 28~34 cm, including the thickness of a whole brick wall (24 cm), the protective layer, the insulation layer and the adhesive layer [26]. On potential application of this research is to reduce environmental noise transmitted into a room via a number of small holes in a wall for ventilation or access purposes, so 30 cm is selected as the depth of the opening. A commercial software product (LMS Virtual Lab 12) is used to validate the analytical model described in Section 2. The element size of the FEM model is 0.007 m, which corresponds to the one-twelfth wavelength of 4000 Hz. The total element number of the FEM model is 1776743. 64 modes of the opening from the (0, 0)th to the (7, 7)th are considered in the calculation with the analytical model. The fluctuation of noise reduction is less than 0.1 dB when modes over (7, 7)th are considered. The cut-off frequency for the plane wave propagation in an infinitely long opening with such a cross section size is 2833 Hz. The amplitude of both primary source and secondary source is 10^{-4} kg·s^{-2}. Fig. 2 shows the calculated sound pressure levels at (−0.1, 0.08, 0.42) m at the transmitted side generated by the primary source at (−0.04, −0.03, −0.1) m and the secondary point source at (0.03, 0, 0.15) m, which agree well with that from the commercial software.

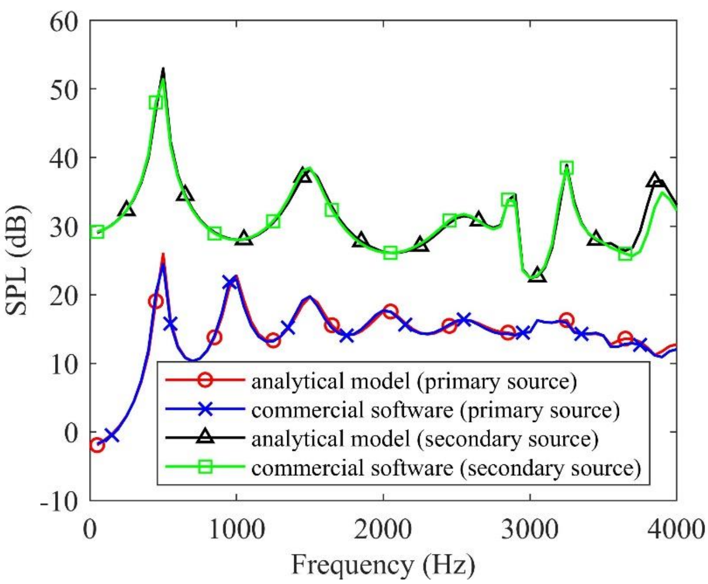

Fig. 2. Comparison of sound pressure level at the measurement point between analytical model and commercial software.

3.2. Effects of secondary sources

The secondary source can be one loudspeaker or a compound source constructed by 2 or 4 loudspeakers. As shown in Fig. 3, the locations of the loudspeakers labelled from 1 to 4 are (0, 0.03, 0.15) m, (0, −0.03, 0.15) m, (0.03, 0, 0.15) m, and (−0.03, 0, 0.15) m, respectively. For a feed-forward system used in practice, some space should be reserved for the reference microphones in front of the secondary sources and error microphones behind the secondary sources. Because the performance of the ANC system does not change significantly if the loudspeakers are at the plane z = 0.12 m or z = 0.18 m, the secondary sources are placed at the plane in the middle of the opening in this paper. All the loudspeakers in the compound control source are driven by the same signal so that a single channel controller is used. In the simulations of this subsection, the transmitted sound power from the opening to the transmitted side is used as the cost function. The parameter β constrains the power of secondary sources and reduces the noise reduction of ANC systems in the simulation, and it is chosen to limit the noise reduction of the system less than 50 dB, which is more consistent with that in practical scenarios.

For the single source configuration (Configuration ANC 1C–1S–W), only Loudspeaker 1 is used; for the compound sources with 2 loudspeakers, Configuration ANC 1C–2S (A)–W uses Loudspeakers 1 and 3 on the adjacent sides while Configuration ANC 1C–2S (O)–W uses Loudspeakers 1 and 2 on the opposite sides; for the compound source with 4 loudspeakers (Configuration ANC 1C–4S–W), all the 4 loudspeakers are used. In the abbreviations, 1C indicates a single channel controller was used, nS indicates n secondary sources were used, and W indicates the transmitted sound power is used as the cost function.

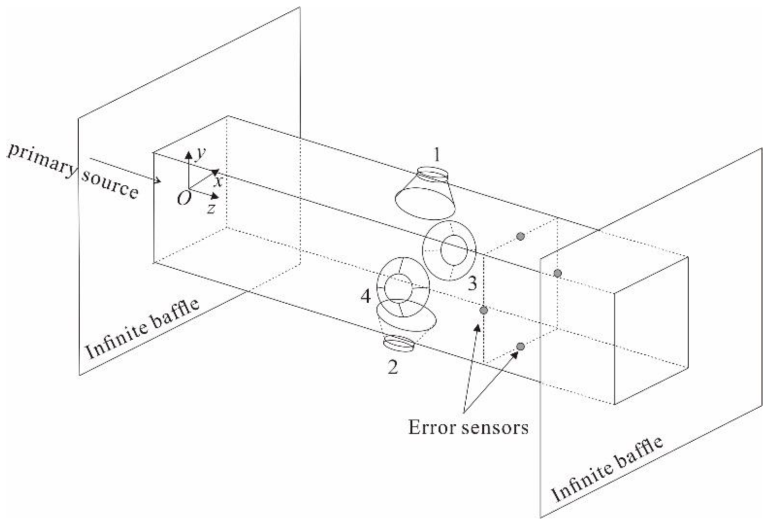

Fig. 3. The scheme of the opening with the secondary sources

A primary source located at (0, 0, 1) m at the incidence side of the opening with a strength of 5 $kg \cdot s^{-2}$ is considered first. The transmitted sound power from the incidence side to the transmitted side without and with ANC is shown in Fig. 4. There is little noise reduction for Configurations ANC 1C–1S–W and ANC 1C–2S (A)–W when the frequency is above 2850 Hz, which is around the cut-off frequency for the plane wave propagation in the opening. The effective control frequency can be extended to higher frequency range with symmetrical configurations, *i.e.*, Configurations ANC 1C–2S (O)–W and ANC 1C–4S–W.

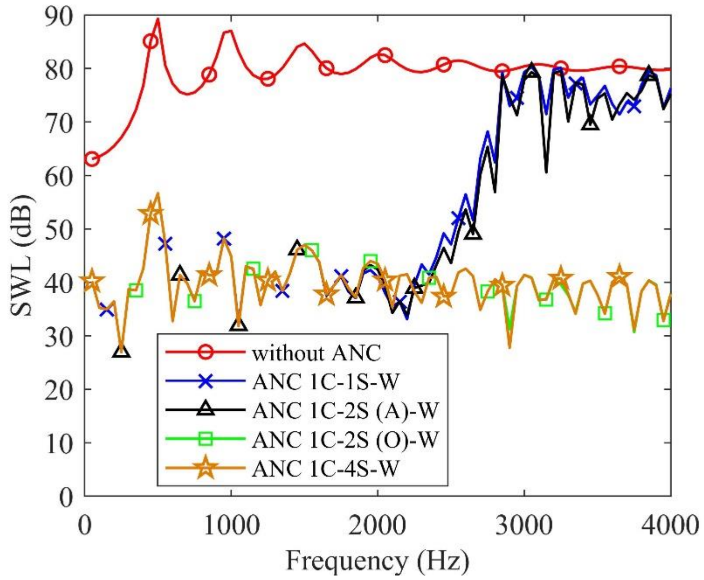

Fig. 4. The transmitted sound power level through a 30×6×6 cm^3 opening with normal incidence

To achieve good noise reduction in the opening, the sound pressure distribution of the secondary sound field needs to match that of the primary sound field. Fig. 5 shows the sound pressure level distribution of the primary sound field and 3 different secondary sound fields at 3000 Hz inside the opening on the cross section at z = 0.24 m. The primary sound distribution at z = 0.24 m is uniform in Fig. 5(a), which indicates almost no high order modes are generated in the opening. The secondary sound distribution at z = 0.24 m generated by a secondary source placed at the midpoint of the side of the wall is shown in Fig. 6. It shows that the distribution of secondary sound field is not uniform, due to the generation of high order modes. Furthermore, the sound pressure on the secondary source's side and the sound pressure of the opposite side have similar amplitude and opposite phase, so the high order modes generated by a secondary source might be suppressed by using another symmetrically arranged secondary source.

The secondary sources in configurations ANC 1C–2S(O)–W and ANC 1C–4S–W are arranged symmetrically to make the amplitudes of high order modes generated by them be lower than that generated by the secondary sources in configurations ANC 1C–1S–W and ANC 1C–2S(A)–W. The secondary sound field of configurations ANC 1C–2S (O)–W and ANC 1C–4S–W matches the primary sound field better so these configurations have better reduction than that of configurations ANC 1C–1S–W and ANC 1C–2S (A)–W.

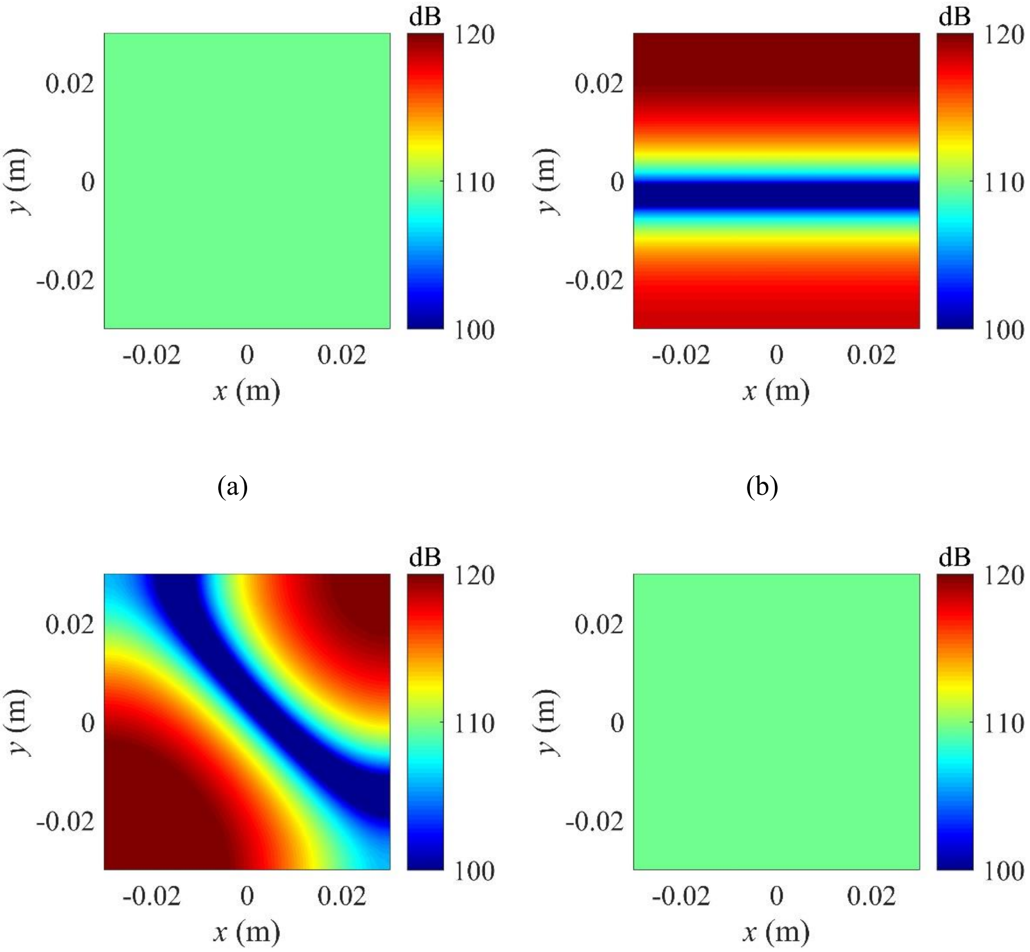

(a) (b)

(c) (d)

Fig. 5. The sound pressure level distribution on the cross section at z = 0.24 m (3000

Hz), (a) the primary sound field, (b) the secondary sound field of Configuration ANC 1C–1S–W, (c) the secondary sound field of Configuration ANC 1C–2S (A)–W, (d) the secondary sound field of Configuration ANC 1C–2S (O)–W.

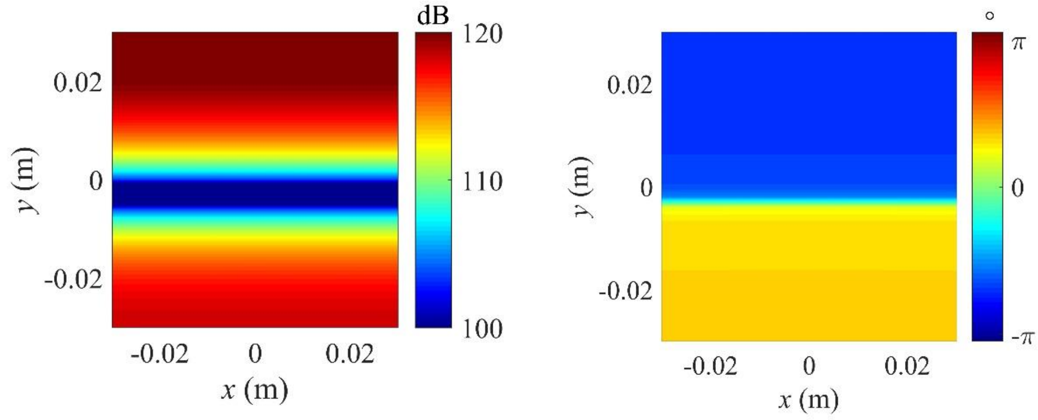

(a) (b)

Fig. 6. The secondary field distribution of ANC 1C–1S–W on the cross section at z = 0.24 m (3000 Hz), (a) sound pressure level, (b) phase.

The primary sound field in Fig. 5 is symmetrical because the primary source is located on the axis of the opening. This is the reason that Configurations ANC 1C–2S (O)–W and ANC 1C–4S–W provide better control than the other two. However, the noise might come from different directions in practical applications. Fig. 7 shows the noise reduction with different types of primary sound fields, which are generated by a primary source located at 1 m away from the opening with normal incidence or oblique incidence with incidence angles (30°, 30°), and 13 primary point sources distributed uniformly on a hemisphere of 4 m radius, having the same center at the incidence side.

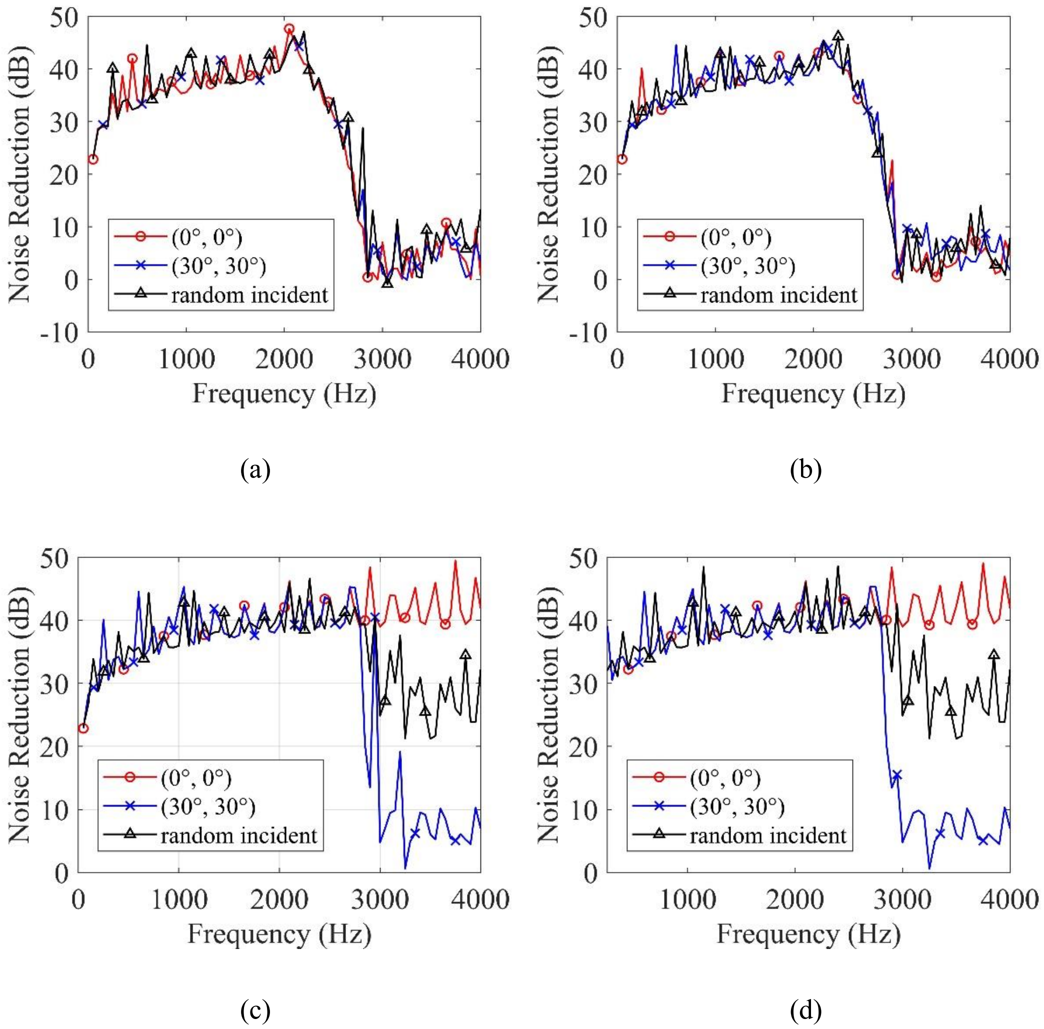

Fig. 7. The NR of the single-channel ANC system for different primary sound fields, (a) Configuration ANC 1C–1S–W, (b) Configuration ANC 1C–2S (A)–W, (c) Configuration ANC 1C–2S (O)–W, (d) Configuration ANC 1C–4S–W.

It is demonstrated that the symmetrical configurations achieve high noise reduction with normal incidence but low noise reduction with oblique incidence above the cut-off frequency. High order modes are generated with oblique incidence above the cut-off frequency and lead to an asymmetrical primary sound field, which cannot match the sound field produced by secondary sources of symmetrical configurations.

For the specific primary sound field generated by 13 primary sources, it has some symmetric components, so the noise reduction performance is between those with normal incidence and oblique incidence.

Multichannel ANC system can be applied to improve the performance of the ANC system with an asymmetrical primary sound field. Fig. 8 shows the noise reduction of systems with 1 channel, 2 channels, and 4 channels for the primary sound field with oblique incidence with incidence angles (30°, 30°). Each channel in Configuration ANC 2C–4S (A)–W controls a pair of loudspeakers on the adjacent sides while each channel in Configuration ANC 2C–4S (O)–W controls a pair of loudspeakers on the opposite sides. In the abbreviations, nC indicates using a n-channel controller. The NRs of the ANC systems with 1 channel or 2 channels are approximately 10-20 dB above the cut-off frequency while the 4-channel system expands upper limit of control to 4000 Hz.

The 4-channel system can theoretical control the (0, 1), (1, 0) and (1, 1) modes in the opening, which have the corresponding modal frequencies of 2833 Hz, 2833 Hz and 4007 Hz. Because the secondary sources can only be located at the midpoints of four walls due to the size of the secondary sources, it is hard for them to generate the (1, 1) mode. For sound with frequency above 4007 Hz, the (1, 1) mode generated by the primary source exists in the opening; however, it cannot be controlled by the secondary sources. As a result, the 4-channel ANC system discussed here can control both the (0, 1) and (1, 0) modes but fails to control the (1, 1) mode, so the upper limit of the control frequency can only be expanded to approximately 4000 Hz, which is close to the corresponding modal frequency of the (1, 1) mode.

In the case of the opening with 0.3 m in depth, high order modes have little influence on the noise reduction below 2700 Hz, but they cannot be completely attenuated when the opening is short, *i.e.*, an opening with 0.1 m in depth, which decrease the noise reduction of configuration with one secondary sound source. With additional numerical simulations, it is shown that the opening depth does affect the performance of the control if number of the secondary sources is not enough. The modal analysis might not be held when the depth is very small (many modes are needed to make the calculation converge), but it can still provide reasonable results when the depth is larger than 0.1 m.

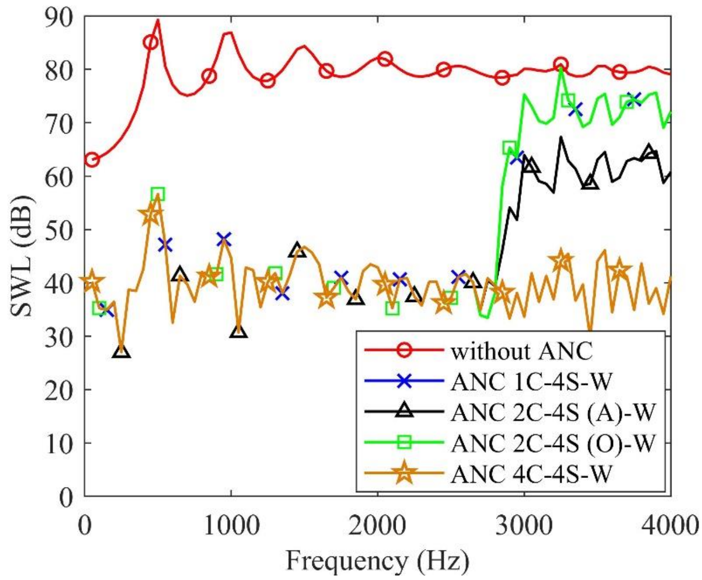

Fig. 8. The transmitted sound power reductions of different channels with 4 loudspeakers for the primary sound field with oblique incidence with incidence angles (30°, 30°).

3.3. Effects of error sensors

The sound power can be obtained by measuring the sound pressure at all locations on an enclosing surface in the far field. In practice, the sum of the squared sound pressure of a limited number of error sensors is usually adopted to estimate the sound power [15]. Three cost functions, *i.e.*, the squared sound pressure of 1 error sensor, the sum of the squared sound pressures of 4 error sensors and transmitted power are compared. With additional numerical simulations, it is shown that the position of error sensors on the same section has little influence on the noise reduction of this active control system. For easy installation in practice, the error sensors are located at the midpoint of four sides of the opening at z = 0.24 m, as shown in Fig. 9. In the case of using 1 error sensor, the error sensor is located at the same side of the activated loudspeaker.

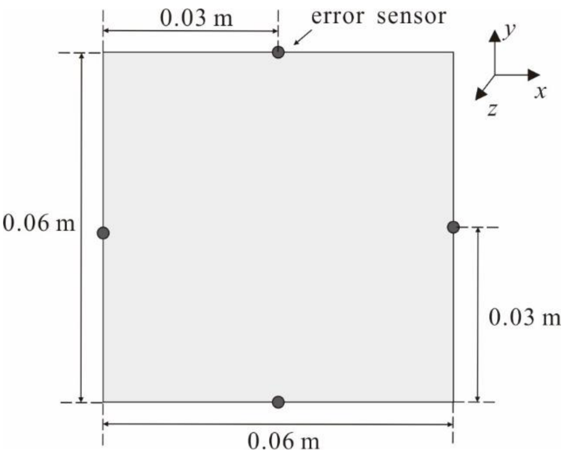

Fig. 9. The locations of the error sensors at z = 0.24 m.

The transmitted sound power reductions of the system with 1 channel and 1 secondary source under the oblique incidence of the primary source with incidence angles (30°, 30°) are shown in Fig. 10. In the abbreviations, nE indicates using n error sensors. The noise reduction of Configuration ANC 1C–1S–1E reduces to less than 20 dB above 2000 Hz because an ANC system with one error sensor cannot control evanescent modes in the opening. By increasing the number of error sensors from 1 to 4, the performance of Configuration ANC 1C–1S–4E approaches to that of Configuration ANC 1C–1S–W.

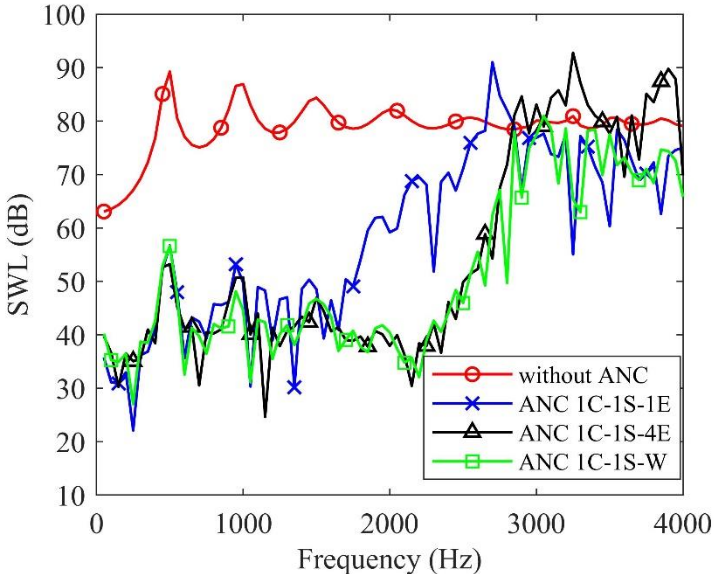

Fig. 10. The transmitted sound power reductions with different cost functions.

4. Experiments

The experiments were conducted in the anechoic chamber of Nanjing University. As shown in Fig. 11, an anechoic box is made of iron plates of 2 mm thickness, and is 120 cm in length, 110 cm in width and 110 cm in depth with an opening sealed by a layer of MDF (medium density fiberboard). One end of a rectangular opening is at the center of the MDF, while the other end of the opening is baffled by two MDF boards measuring 110 cm in length, 100 cm in width and 3.6 cm in depth. The length, width and depth of the opening are 6 cm, 6 cm and 31.8 cm, respectively. Since the four walls of the anechoic box are filled with glass wool of 10 cm thickness and the bottom is fixed with 50 cm sound-absorption wedge with the length of 40 cm, the inside of the anechoic box is considered as a semi-infinite space adjoined to the transmitted side of the opening. The thickness of the MDF boards is 1.8 cm and the surface density is approximately 30 kg·m^{-2}. The anechoic chamber is used as the incidence side and the primary source is located at (0.25, 0, −0.482) m, which is driven by a B&K Pulse 3160 LAN-Xi to generate tonal signals.

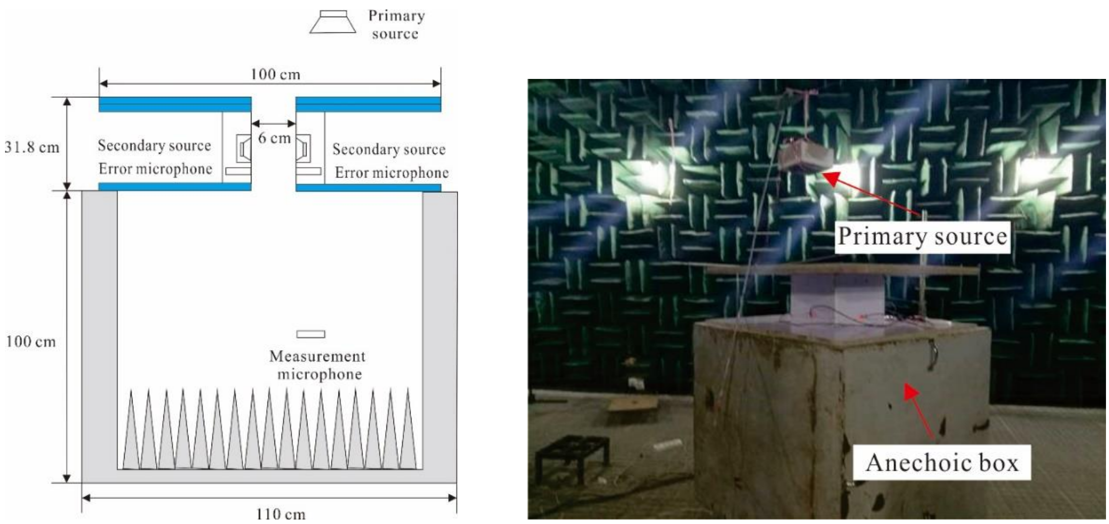

(a) (b)

Fig. 11. Experimental setup, (a) schematic of the opening and the anechoic box, (b) panoramic view of the anechoic chamber, the opening and the anechoic box.

Three ANC systems, *i.e.*, a single-channel ANC system with 1 error sensor (Configuration ANC 1C–1S–1E), a single-channel system with 4 error sensors (Configuration ANC 1C–1S–4E) and a 4-channel system with 4 error sensors (Configuration ANC 4C–4S–4E) are implemented at the opening. Four secondary sources are located inside the opening at (0.03, 0, 0.168) m, (−0.03, 0, 0.168) m, (0, 0.03, 0.168) m, and (0, −0.03, 0.168) m and the secondary source at (0.03, 0, 0.168) m is used in the Configurations ANC 1C–1S–1E and ANC 1C–1S–4E. Four error microphones are located at (0.03, 0, 0.258) m, (−0.03, 0, 0.258) m, (0, 0.03, 0.258) m, and (0, −0.03, 0.258) m and the error sensor at (0.03, 0, 0.258) m is used in the Configuration ANC 1C–1S–1E. The measurement microphone is placed in the anechoic box, at (0, 0.02, 0.688) m. A commercial ANC controller (TigerANC-II Lite, Antysound) embedded with the multichannel FxLMS algorithm is used in the experiments with a sampling frequency of 16 kHz. The electrical signal driving the primary source is also fed to the controller as the reference signal. The measurement frequencies are from 200 Hz to 4000 Hz with steps of 50 Hz.

Comparisons between the sound pressure level of the simulation and the experiment at the error microphone located at (0.03, 0, 0.258) m and the measurement microphone are shown in Fig. 12. General trends of the measured sound pressure levels agree well with the simulation results. Factors such as the damping of the baffle, the transmitted sound through the baffle, the diffracted wave of the finite baffle, the reflected wave at low frequency and the directivity of the loudspeakers at high frequency may cause the difference between two curves.

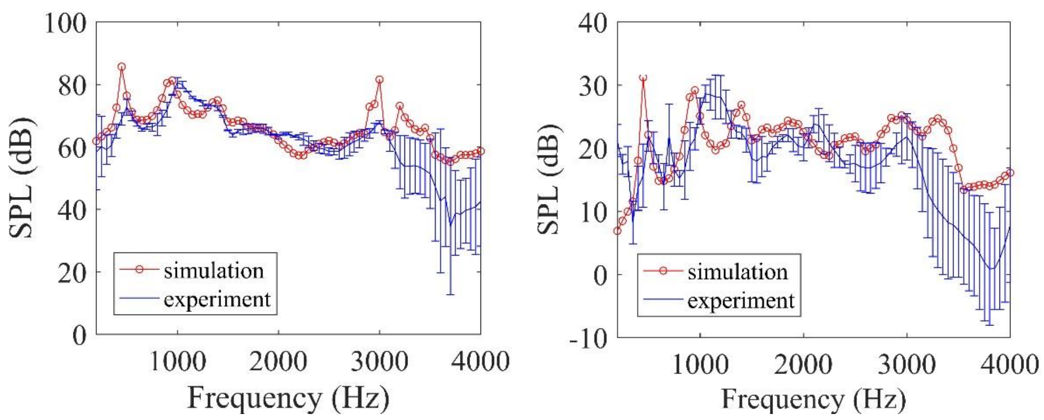

(a) (b)

Fig. 12. The comparison between analytical and experimental sound pressure level, (a) the error microphone, (b) the measurement microphone.

Fig. 13 shows the sound power level with and without active control at the measurement microphone for tonal signals from 200 to 4000 Hz with steps of 50 Hz. The solid red line with circular markers denotes the sound pressure level of measurement microphone in the free-field respect to the frequency, and the solid blue line with cross markers denotes measurements without the ANC system. The difference of these two lines shows the passive sound insulation ability of the opening at the measurement point. The solid black line with triangle markers shows that Configuration ANC 1C–1S–1E achieves more than 10 dB NR at most frequencies below 1200 Hz. The solid green line with square markers shows that Configuration ANC 1C–1S–4E achieves more than 10 dB NR at most frequencies below 2750 Hz. Configurations ANC 1C–1S–1E and ANC 1C–1S–4E are measured up to 2800 Hz, corresponding to their upper limit of control range. The performance of the system with 4 error sensors is better than that of the system with 1 error sensor above 2000 Hz, which is in line with the simulation results.

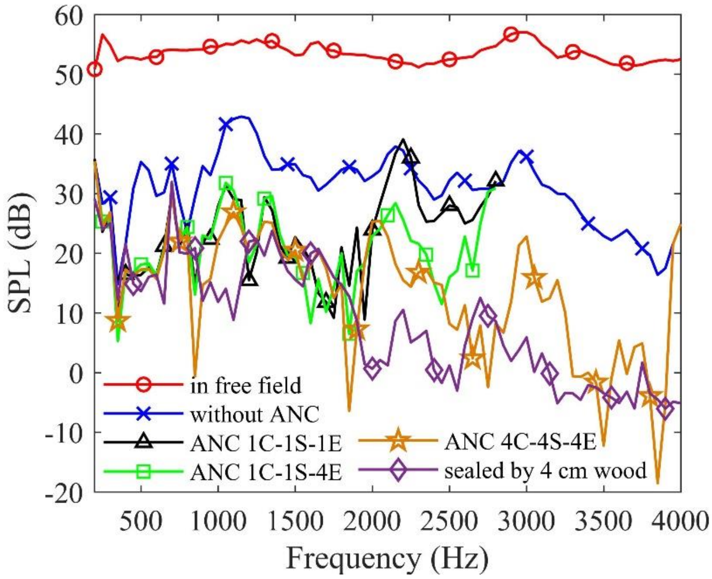

Fig. 13. The performances of different ANC systems at the measurement microphone (Configurations ANC 1C–1S–1E and ANC 1C–1S–4E are measured up to 2800 Hz).

The solid yellow line with pentagram markers shows that Configuration ANC 4C–4S–4E achieves more than 10 dB NR at most frequencies below 3900 Hz. The cut-off frequency of the anti-aliasing filter embedded in the controller is 3900 Hz and restricts the performance of Configuration ANC 4C–4S–4E beyond 4000 Hz. Comparison between the solid black line with triangle markers, the solid green line with square markers and the solid yellow line with pentagram markers indicates that the measured upper frequency limits of control for the single-channel system and the 4-channel system are 2750 Hz and 3900 Hz respectively, which is in line with the simulation results. The solid purple line with diamond markers denotes the sound pressure level at the measurement point with the opening blocked by 4 cm thick wood so it represents the sound insulation ability of the MDF baffles. Comparison between the solid black line with triangle markers, the solid green line with square markers, the solid yellow line with pentagram markers and the solid purple line with diamond markers indicates that the maximal NR of the ANC system embedded in the opening is limited by the passive sound insulation ability of the MDF baffles below 1950 Hz except frequencies near 1100 Hz.

5. Conclusions

This paper investigates the active control of sound transmission through an opening of 6 cm by 6 cm. An analytical model developed with the modal expansion method is first verified with a commercial numerical software product, and then the effects of different secondary source and the error sensor strategies are compared numerically for different types of primary sound fields. The numerical results demonstrate that implementing active control in small openings can increase the upper frequency limit of control to 4000 Hz. By analyzing the sound field in the opening, it is found that the upper frequency limit of control depends on the eigen frequency of the acoustic modes of the opening as well as the secondary source and error sensing strategies. The experiments were designed to demonstrate the practical feasibility of the active control system in a small opening.

For many practical noise control scenarios which have both noise reduction and ventilation requirements, a number of such openings can be made in the enclosure walls to provide effective broadband noise control. Further work includes implementation of time domain algorithms with real reference sensors and studying the effects of thin walls and interaction of multiple openings.

ACKNOWLEDGEMENTS

This work was supported by National Science Foundation of China [grant numbers 11874218, 11874219].

REFERENCES

[1] C. Bouwkamp, Diffraction theory, Rep. Prog. Phys. 17 (1954) 35–100.

[2] G. Wilson, W. Soroka, Approximation to the diffraction of sound by a circular aperture in a rigid wall of finite thickness, J. Acoust. Soc. Am. 37 (1965) 286–297.

[3] A. Sauter, W. Soroka, Sound Transmission through Rectangular Slots of Finite Depth between Reverberant Rooms, J. Acoust. Soc. Am. 47(1) (1970) 5–11.

[4] F. Sgard, H. Nelisse, N. Atalla, On the modelling of diffuse field sound transmission loss of finite thickness apertures, J. Acoust. Soc. Am. 122 (1) (2007) 302–313.

[5] N. Trompette, J. Barbry, F. Sgard, H. Nelisse, Sound transmission loss of rectangular and slit-shaped apertures: experimental results and correlation with a modal model, J. Acoust. Soc. Am. 125(1) (2009) 31–41.

[6] M. Francesco, On the sound absorption by openings in rooms (L), J. Acoust. Soc. Am. 132(5) (2012) 2951–2954.

[7] K. Jun, H. Eom, Acoustic scattering from a circular aperture in a thick hard screen, J. Acoust. Soc. Am. 98(4) (1995) 2324–2327.

[8] H. Park, H. Eom, Acoustic scattering from a rectangular aperture in a thick hard screen, J. Acoust. Soc. Am. 101(1) (1997) 595–598.

[9] J. Horner, K. Peat, Higher mode sound transmission from a point source through a rectangular aperture, J. Acoust. Soc. Am. 129(1) (2011) 5–11.

[10] J. Poblet-Puig, A. Rodríguez-Ferran, Modal-based prediction of sound transmission through slits and openings between rooms, J. Sound Vib. 335(5) (2013) 1265–1287.

[11] W. Rdzanek, Sound scattering and transmission through a circular cylindrical aperture revisited using the radial polynomials, J. Acoust. Soc. Am. 143, (2018) 1259–1282.

[12] C. Field, F. Fricke, Theory and applications of quarter-wave resonators: A prelude to their use for attenuating noise entering buildings through ventilation openings, Appl. Acoust. 53(1-3) (1998) 117–132.

[13] J. Kang, M. Brocklesby, Feasibility of applying micro-perforated absorbers in acoustic window systems, Appl. Acoust. 66(6) (2005) 669–689.

[14] S. Ise, Theory of acoustic impedance control for active noise control, in: Proceedings of Inter-noise, Yokohama, Japan, 1994.

[15] B. Kwon, Y. Park, Interior noise control with an active window system, Appl. Acoust. 74(5) (2013) 647–652.

[16] B. Lam, C. Shi, D. Shi, W.-S. Gan, Active control of sound through full-sized open windows, Build. Environ. 141 (2018) 16–27.

[17] H. Huang, X. Qiu, J. Kang, Active noise attenuation in ventilation windows, J.

Acoust. Soc. Am. 130(1) (2011) 176–188.

[18] S. Wang, J. Tao, X. Qiu, Performance of a planar virtual sound barrier at the baffled opening of a rectangular cavity, J. Acoust. Soc. Am. 138(5) (2015) 2836–2847.

[19] S. Elliott, J. Cheer, L. Bhan, C. Shi, W.-S. Gan, A wavenumber approach to analysing the active control of plane waves with arrays of secondary sources, J. Sound Vib. 419 (2018) 405–419.

[20] B. Lam, S. Elliott, J. Cheer, W.-S. Gan, Physical limits on the performance of active noise control through open windows, Appl. Acoust. 137 (2018) 9–17.

[21] K. Sha, J. Yang, W. Gan, A simple calculation method for the self- and mutual-radiation impedance of flexible rectangular patches in a rigid infinite baffle, J. Sound Vib. 282(1) (2005) 179–195.

[22] R. Mangiarotty, Acoustic radiation damping of vibrating structures, J. Acoust. Soc. Am. 35(3) (1963) 369–377.

[23] P. Morse, K. Ingard, Theoretical Acoustics. McGraw Hill, New York, 1968.

[24] P. Nelson, S. Elliott, Active control of sound. Academic press, London, 1991.

[25] A. Berry, X. Qiu, C. Hansen, Near-field sensing strategies for the active control of the sound radiated from a plate, J. Acoust. Soc. Am. 106(6) (1999) 3394.

[26] GJBT-1340, National architectural standard design atlas 15J101 15G612: Brick wall building, structure and construction. China planning press, Beijing, 2015 (in Chinese).